

# Passive Steering of Miniature Walking Robot using the Non-Uniformity of Robot Structure

Jinhong Qu

Dept. of Mechanical Engineering  
University of Michigan  
Ann Arbor, MI, USA  
jinhongq@umich.edu

Clark B. Teeple

Dept. of Mechanical Engineering  
University of Michigan  
Ann Arbor, MI USA  
cbteeple@umich.edu

Buyi Zhang

Dept. of Mechanical Engineering  
University of Michigan  
Ann Arbor, MI USA  
buyiz@umich.edu

Kenn R. Oldham

Dept. of Mechanical Engineering  
University of Michigan  
Ann Arbor, MI, USA  
oldham@umich.edu

**Abstract**—This paper discusses the steering of a miniature, vibratory walking robot taking advantage of the robot's structural non-uniformity. Non-uniformity from fabrication and assembly can be detrimental to performance of miniature robots, but its potential for modifying robot locomotion is discussed in this work. A 3-centimeter-wide piezoelectric robot is described for the study of steering opportunities. This includes turning behavior that occurs away from resonance due to leg asymmetries and shuffling behavior caused by lateral motion of the actuators. Finite Element Analysis and beam theory are used to explain the resonances of the designed structure. The parameter variances are studied and experimentally validated, to illustrate the variability of locomotion effects emerging across the robot legs. Further explanation of the robot dynamics helps to determine possible mechanisms for steering, with rotational turning motion around resonance explainable with a previous dynamic model, and some candidate explanations for shuffling examined. The motion of the robot is recorded within the frequency range of 1.2 to 4.6 kHz, within which both turning and shuffling are observed in addition to longitudinal motion.

**Keywords**—Miniature robots, Steering, Structural Dynamics, Finite Element Analysis.

## I. INTRODUCTION

Miniature walking robots [1, 2] at the scale of several centimeters or smaller have exhibited increasing capacity for moving rapidly under certain actuation schemes. Multiple transduction and actuation mechanisms have succeeded in realizing terrestrial locomotion at these small scales [3-6]. Based on an understanding of their actuators and linear and/or nonlinear appendage dynamics, associated dynamic models of full robot locomotion have been developed. Dynamic models and simulated gaits have been most accurate around resonances generated by the elastic features that are often present in small-scale robots [2, 7]. However, control of robot motion is desired beyond just the speed of forward and backward motion. Steering these robots [6, 8-10] over various surfaces is also important for potential future applications, but this has received comparatively less attention among small-scale, terrestrial legged robots. Murthy et al. [6], as one example, fabricated a walking microrobot with six legs, which could be steered with different actuation signals to the left and right legs. Donald et al. [9] designed and tested a robot as small as 250  $\mu\text{m}$  in length. The robot was designed with a steering arm, which could turn

the robot on the walking surface. Dharamawan et al. [8] presented a centimeter-scale miniature robot with single unimorph PZT actuator. Steering was realized by applying various actuation frequency to the asymmetrically designed robot legs. Goldberg et al. [10] introduced the open-loop control of HAMR, a small-scale robot, with foot phase control, realizing both forward motion and turning at various frequencies. These works all either required extra components for steering or were designed for locomotion specific to certain substrates. At slightly larger scales, aerodynamics [11] and tails [12] have been proposed to aid steering of small legged robots.

In this paper, frequency-based steering of a miniature, vibration-driven legged robot is examined. Steering is defined as robot motion that predictably deviates from the ideal forward and backward direction of the robot. The forward direction is defined as the principle direction of actuator vibration in the plane of the walking surface. Steering is then divided into two types: turning and shuffling. Turning is defined as the robot motion that changes the forward direction of robot, also meaning that the robot is rotating about its vertical axis. Shuffling is robot motion that is not in the forward direction but without change in robot orientation.

A detailed dynamic model [2] including body dynamics, compliant dynamics, and contact dynamics has been previously derived by the authors to explain the straight motion of robots based on compliant leg structures experiencing vibration in a modal elastic manner. This model placed particular emphasis on the relationship between robot speed and actuation parameters and/or ground conditions. The model will not be reproduced in full in this paper due to space. Instead, this paper will summarize how that model helps to explain the turning of the robot when non-uniformity of the robot's structure, particularly its legs, is accounted for, then examine some observed shuffling phenomena that are outside the scope of the prior model. Dharamawan et al. [8] also studied the relationship between resonance modes of actuators and locomotion, to explain steering observed experimentally in a 4-leg robot with one unimorph actuator. That robot was close to 50 cm in length. Otherwise, limited attention has been paid to the connection between robot steering and structural non-uniformities, perhaps because it is believed that the non-uniformity will disappear or at least become less notable if the fabrication resolution is improved during technology development. However, with better understanding of robot

Funded by National Science Foundation (NSF)

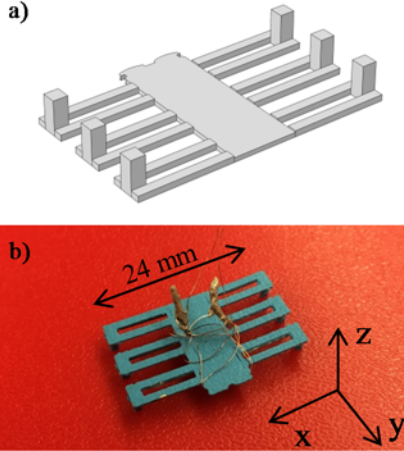


Fig. 1. (a) The 3D model of robot design, shown upside down; and (b) a photo of the robot after assembly.

non-uniformity, it may be possible to take further advantage of such features for the control of robot motion, to achieve steering by carefully selecting simple actuation input that cause the motion bias, instead of separate control of each leg.

This paper is organized as follows: Section II briefly introduces the architecture of the robot. Then the robot leg resonance is presented with experimental measurements, with comparison to results from finite element analysis (FEA) and Bernoulli beam theory. Parameter variance is also evaluated to show how large the diversity of robot leg dynamics may be. The Section IV discusses application of a dynamic model and compares observations from the model to measurements of the steering at different frequency. Section V draws some conclusions and identifies opportunities for future study.

## II. ROBOT ARCHITECTURE

A six-leg miniature robot is designed and assembled to study the steering of miniature robots. The robot structure is 3D-printed with polylactic acid (PLA), as shown in Fig. 1 (a). Each robot leg is a double-beam structure with a cuboid attached to its end. A unimorph lead-zirconate-titanate piezoelectric actuator (PZT, Naval type VI) is epoxied to the bottom of one beam in each leg. The intentional asymmetry of the actuator arrangement produces vibration of the robot legs in both vertical and lateral directions, to overcome both gravity and friction. The six total actuators in the robot are wired for a nominal tripod gait, in which three actuators as a group are out-of-phase to the other group based on polarity of the PZT. Therefore, the electrical connections are pre-determined, and the robot can be actuated with a single actuation channel. An assembled robot is shown as Fig. 1 (b).

The robot design parameters and their values are shown in Table I. The entire footprint of the robot is less than  $6 \text{ cm}^2$ , and the mass is less than 400 mg. In this paper, the direction terminology is defined here and described in these terms through the paper:

1) *longitudinal direction (y-direction)*: the direction along the longitude side of the robot body; the nominal robot motion is designed to be in this direction. Forward and backward are used to describe the motion in this direction

2) *lateral direction (x-direction)*: the direction along the longitude side of the robot leg, labeled with left and right

3) *vertical direction (z-direction)*: the direction along the direction of gravity. The gravitational direction is defined as the negative vertical direction.

TABLE I. ROBOT DESIGN PARAMETERS

| Feature                     | Description                                 |
|-----------------------------|---|
| Mass                        | 379 mg                                      |
| Actuators                   | 6 Unimorph PZT                              |
| Actuation phase             | Tripod                                      |
| Leg design                  | Double beam                                 |
| PLA density ( $\rho$ )      | $1.19 \times 10^3 \text{ kg/m}^3$           |
| PLA Young's modulus ( $E$ ) | $3.5 \times 10^9 \text{ Pa}$                |
| Dimension                   | Value                                       |
| Body Length                 | 16.5 mm                                     |
| Actuator                    | $11 \times 0.95 \times 0.12 \text{ mm}^3$   |
| Foot                        | $1.46 \times 1.53 \times 3.35 \text{ mm}^3$ |
| Leg                         | $9.43 \times 1.17 \times 0.54 \text{ mm}^3$ |

## III. ROBOT LEG RESONANCE

Because actuating lightly-damped elastic leg structures around resonance can help amplify the motion amplitude of piezoelectric actuators, the legs' resonant frequencies are estimated with FEA and beam theory and then compared with experimental results. Limited fabrication resolution and repeatability lead to parameter variance and thus different resonant frequencies or amplitudes among legs. Some analysis is done in this section to predict the magnitude of variance in motion across the legs and assess the major factors affecting this variance.

### A. Finite Element Analysis (FEA)

The design of a robot leg is first analyzed in COMSOL Multiphysics [13] to simulate the first several resonant modes. The leg geometry is from the robot design and material properties are collected from the 3D printer data manual. As shown in Fig. 2, the first resonant mode shape is a vertical motion at 1436 Hz, and the second mode shape is a tilting mode at 3977 Hz. Though the first mode will be referred to as the vertical mode, motion in the longitudinal direction still exists, which can be used to generate motion in-plane. The second mode is a tilting mode, which has limited vertical motion. However, if the actuation signal is large, this mode can move the robot rapidly as long as the small vertical force can bounce the robot off the ground.

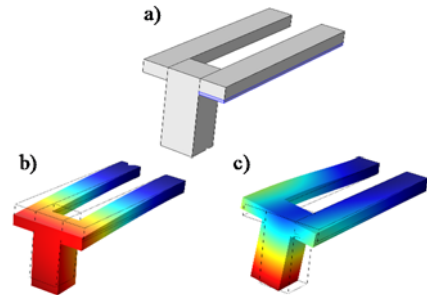


Fig. 2. Finite Element Analysis of (a) the double-beam robot leg structure; (b) the first resonance is a vertical mode at 1436 Hz and (c) the second resonance is a tilting mode at 3977 Hz.

## B. Beam Theory

Beam theory can also explain the vibration of a cantilever beam. The resonant frequency of such a beam is:

$$f = \frac{\alpha^2}{2\pi} \sqrt{\frac{Et^2}{12\rho L^4}} \quad (1)$$

in which  $\alpha$  is a coefficient calculated by solving boundary conditions, frequently as a trigonometric function;  $E$  is the Young's Modulus;  $\rho$  is the density per unit length;  $t$  and  $L$  are the thickness and length of the beam accordingly.

$\alpha$  is assumed to be a constant with unchanged boundary condition of the robot, though variance in dimensions and material properties may change the  $\alpha$  value slightly. The  $\alpha$  value of standard cantilever is used. Using parameters listed in Table I, along with the Young's modulus ( $3.5 \times 10^9$  Pa) and the density ( $1.19 \text{ kg/m}^3$ ) of PLA, the first resonant frequency of one beam of robot leg is 1676 Hz from calculation. While the geometry and the boundary conditions of the actual double-beam leg are more complex than a simple cantilever, the reasonably close agreement suggests that the beam theory result may serve as a source of reference for assessing the sensitivity of dynamic variability to fabrication variability. The calculated frequency is higher than FEA, possibly because of the rigid connection between two beams.

## C. Parameter Variation

Based on the beam theory, the influence of different design parameters on the frequency can be approximated by taking partial derivatives of (1). As mentioned above, it is not fully accurate to use the single beam boundary condition to solve the double-beam problem, but the change of boundary conditions will predominantly affect the coefficient in the front of the solution, not the parameters included in the equation. The expressions for the frequency sensitivity of selected design and/or fabrication parameters are:

$$\delta_\omega = \begin{cases} 2 \frac{\alpha^2}{2\pi} \sqrt{\frac{Et^2}{12\rho L^4}} E\% \\ -\frac{\alpha^2}{2\pi} \sqrt{\frac{Et^2}{12\rho L^4}} \rho\% \\ \frac{\alpha^2}{2\pi} \sqrt{\frac{Et^2}{12\rho L^4}} t\% \\ -2 \frac{\alpha^2}{2\pi} \sqrt{\frac{Et^2}{12\rho L^4}} L\% \end{cases} \quad (2)$$

in which  $\delta_\omega$  is the change of frequency and  $E\%$ ,  $\rho\%$ ,  $t\%$ , and  $L\%$  are the percentage changes of Young's Modulus, PLA density, beam thickness, and beam length accordingly. Results in (2) can indicate how large variance in resonant frequency of individual legs may be for a given fabrication technology. As shown in Table II, the length of beam is the parameter with the largest influence on the resonant frequency.

In practice for the robot, the density and the Young's modulus of PLA have the largest variance given the 3D printing fabrication resolution. From (1) and (2), as might be expected from standard fractional analysis, 1% change in thickness will leads to 1% change in the resonant frequency,

TABLE II. SENSITIVITY OF RESONANT FREQUENCY PER PERCENTAGE CHANGE OF ROBOT DESIGN PARAMETERS

| Feature | Sensitivity                  |       |
|---------|------------------------------|-------|
|         | per percent parameter change | ratio |
| $E$     | 8.38 Hz/%                    | 0.5   |
| $\rho$  | -8.38 Hz/%                   | -0.5  |
| $t$     | 16.76 Hz/%                   | 1     |
| $L$     | -33.52 Hz/%                  | -2    |

and 1% change in Young's modulus, density, and beam length will cause 0.5%, 0.5%, and 2% change to the value of resonant frequency. The measured resolution of dimensional parameters is around 5%, and the variability of printed density and Young's modulus can be greater than 10%. Therefore, the overall change in resonant frequency may vary from 10 to 20%

## D. Measurement

After analysis, the leg motions of the robot described in section II are measured experimentally during vibration in air. The frequency difference caused by parameter variance is observed around resonance. Fig. 3 (a) shows that the first resonance is around 1.4 kHz, within a 10% range among the legs. Resonant frequency prediction from FEA was 1436 Hz and from beam theory was 1676 Hz. The second resonance is about 4 kHz, close the 3977 Hz predicted by FEA, but with greater variation in amplitude from leg to leg. This greater variance may be caused by limited assembly resolution.

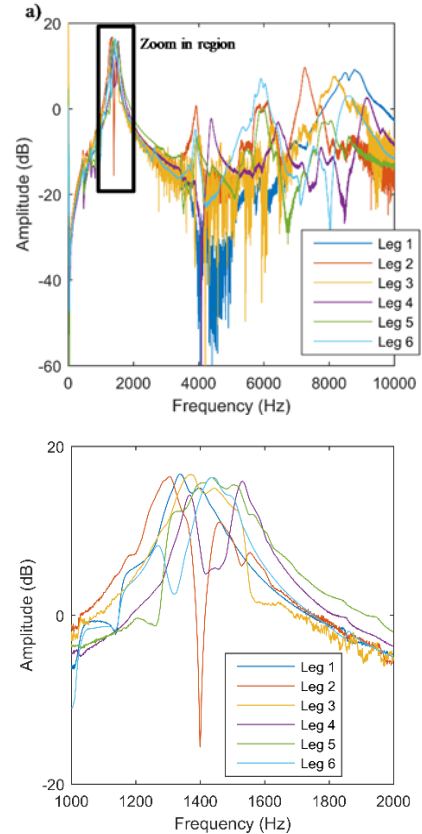


Fig. 3. (a) The frequency response of all 6 robot legs from DC to 10 kHz, and (b) the zoomed-in plot of the region of 1 to 2 kHz, showing the peak frequency distributed between 1.30 to 1.54 kHz.

Detailed frequency response near the first resonance (Fig. 3 (b)) shows measured resonances from 1.30 kHz to 1.54 kHz across the legs. This 10% variance of resonant frequency is consistent with fabrication uncertainty analyzed by the simple beam bending methods; for the robot used in this paper, the variance of leg thickness is about 5% caused by the 3D printing resolution. Smaller miniature robots may suffer from even greater resolution errors. Based on these results, the achievable steering with this level of variance is worth further evaluation.

#### IV. DYNAMIC MODEL

The influence of identified variation in leg dynamics has been analyzed using a previously-developed dynamic model. The dynamic model described by the authors in [1, 2] is effective in explaining trends of robot forward and backward speed as a function of input frequency and voltage. With information on individual leg dynamics, that model can also predict the rate of robot rotation or turning. However, lateral shuffling motion can also occur, which cannot be described using that earlier model as only leg motion in the y-z plane (as defined in Fig. 1 (b)) is included. It is worth noting that as robot size decreases, the margin of error on angular rotation rate increases substantially due to random influences of ground variability and foot-ground impact timing variations. The motion of an 80-mm robot described in those papers was slower and smoother than that of the 30-mm robot examined here; turning of larger robot was also found to be more predictable with the dynamic model. Shuffling was not observed with the larger robot, however. Shuffling is anticipated to be predictable if inclusion of the 6<sup>th</sup> degree of freedom of the robot foot (lateral motion in the x-axis) is accounted for, with the following section presenting a basic approximation of turning and shuffling behaviors.

##### A. Analytical Estimate

As noted above, longitudinal (y-axis) body motion and turning can be simulated with the authors' existing dynamic model. The robots described here are designed for forward locomotion. If the robot legs are non-uniform, though, and the front legs provide more vertical force or phase of vertical to longitudinal foot motion varies with frequency, the robot may move backward; such behavior is observed in both simulation and experiments. Turning, however, arises in simulation only if there is imbalance in motion between left and right legs. Similar to certain variations in longitudinal motion speed caused by imbalance between front and rear legs, the imbalance between legs on either side may rotate the robot body because the longitudinal portion of the actuation force is non-uniformly distributed in time and amplitude.

Fig. 4 and Fig. 5 shows a sample simulation of robot motion when actuation frequency is 1.4 kHz. Fig. 4 shows the robot leg motion when the leg non-uniformity is considered. The motion varies dramatically from leg to leg though the difference is only 5% in leg parameters. In Fig. 5, the simulation of robot body motion is a slightly right turn in the reverse direction. This simulation shows the possibility of turning with robot non-uniformity around the resonance, in this case near the first resonance.

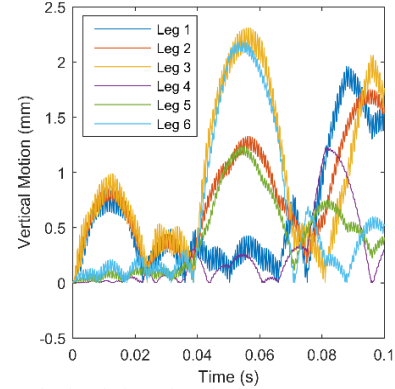


Fig. 4. Sample simulation of vertical feet movement at 1.4 kHz: the motion of 6 robot legs shows varying numbers of impacts and duration in contact with ground based on variation in parameters describing leg

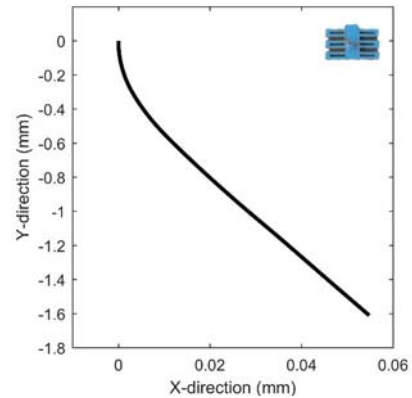


Fig. 5. Sample simulation of robot in-plane motion at 1.4 kHz from position (0,0): the motion of the center of mass of robot body is shown, which is turning right slightly in the backward direction

Modeling shuffling motion requires accounting for lateral (x-axis) motion of the robot feet and body, previously neglected in dynamic modeling due to nominally small amplitude from cantilever-like leg bending in the x-z plane. However, for the robot in this work, shuffling is frequently observed experimentally, motivating further analysis.

In small deflection beam theory, the deflection of the beam tip is calculated in the vertical direction only. However, such deflection will bend the beam in the lateral direction as well, though with small amplitude. A simple approximation for lateral tip displacement in the robot body frame is:

$$\delta_x = \delta_y \cos(\theta) = \delta_y^2 / L \quad (3)$$

in which  $L$  is the length of a beam,  $\theta$  is the angle between the original and deflected direction of robot leg,  $\delta_x$  and  $\delta_y$  are the displacement in lateral and vertical direction, accordingly. Consider then the prototype robot, with an actuation amplitude of 40 V: the robot leg can deflect around 50  $\mu\text{m}$ , so the displacement in lateral direction is around 0.25  $\mu\text{m}$  and the bending angle is about 0.3° from derivation. The off-axis displacement is small enough to be neglected in most conditions, which is also the assumption in our previous dynamic model. In this example, this deflection will be accumulated to a motion of 1.25 mm/s at 2.5 kHz

## B. Experimental Results

The robot motion is video recorded and then analyzed with software to extract motion information. Fig. 6 shows some sample frames of the videos, including movement straight backwards, a turn to the left, and shuffling to the left.

Fig. 7 plots nine robot trajectories together, showing all robot motion types measured at different frequency within 1.2 to 4.6 kHz; Table III lists the motion type and speed observed at various frequency. The speed of longitudinal motion could be up to 5 body lengths per second around the second resonant frequency (3.9 kHz). The power cord may influence the robot motion, so it is inaccurate to measure the speed after the power cord has tension force due to the position change of robot. Only the beginning portion of the measurement is used to calculate the robot speed, as before each test run the power cord is released to remove the tension.

The entire measurement is divided into three frequency ranges, around the first resonance, between resonances, and around the second resonance. First, the robot motion is in the longitudinal direction near the first resonance. The first mode shape of the robot legs dominates motion in this frequency range, with direction determined by slight variations in phase.

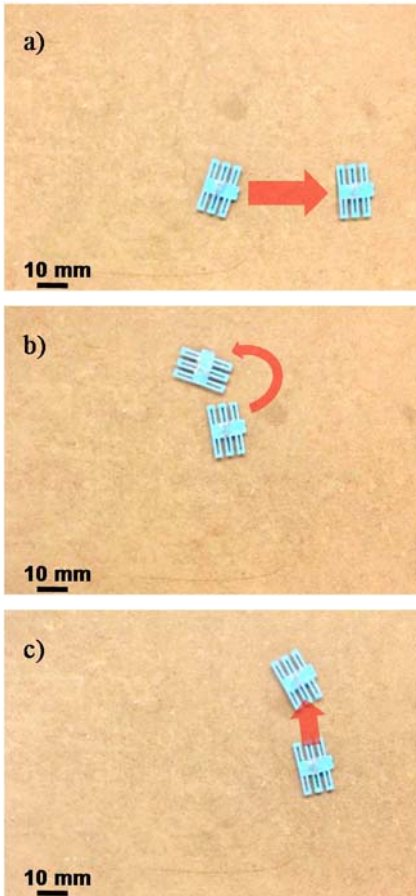


Fig. 6. Sample frames of robot motion on a smooth wood surface: (a) straight backward motion at 1.6 kHz, robot position at 0 and 4s; (b) turning left in backward direction at 2.1 kHz, robot position at 0 and 8s; (c) shuffling left at 2.5 kHz, robot position at 0 and 8s

TABLE III. ROBOT MOTION TYPE AND SPEED AT DIFFERENT ACTUATION FREQUENCY

| Frequency | Motion Type            | Speed                |
|-----------|------------------------|----------------------|
| 1.2 kHz   | Straight forward       | $4.2 \pm 2.5$ mm/s   |
| 1.6 kHz   | Straight backward      | $17.5 \pm 6.7$ mm/s  |
| 2.1 kHz   | Turning left (backing) | $10.6 \pm 5.6$ mm/s  |
| 2.5 kHz   | Shuffle left           | $50.2 \pm 28.1$ mm/s |
| 2.6 kHz   | Straight backward      | $18.4 \pm 5.8$ mm/s  |
| 3.9 kHz   | Straight forward       | $51.3 \pm 14.3$ mm/s |
| 4.1 kHz   | Shuffle left           | $24.5 \pm 10.8$ mm/s |
| 4.2 kHz   | Straight forward       | $9.9 \pm 5.2$ mm/s   |
| 4.6 kHz   | Shuffle right forward  | $33.0 \pm 9.0$ mm/s  |

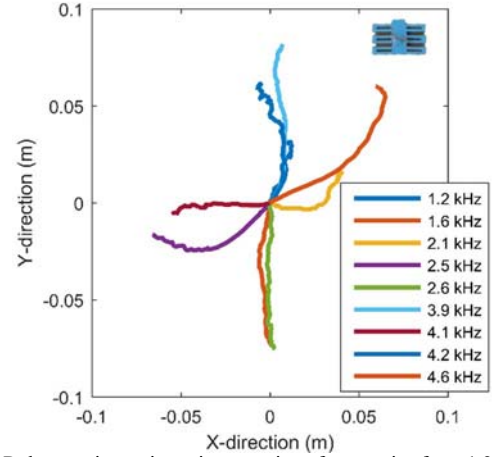


Fig. 7. Robot motion trajectories at various frequencies from 1.2 kHz to 4.6 kHz. Straight motion, turning, and shuffling are all observed experimentally.

Robot motion is more varied between the resonant frequencies (1.4 kHz and 4.0 kHz). Within this frequency range, this example robot has a strong tendency to steer left. Observing the fabrication outcome, the right legs had a better fabrication finish, and resulting larger motion amplitude with identical actuation inputs. In this range, small change in relative phases of the individual leg's modal contributions, combining effects from multiple resonances, can cause major changes in locomotion behavior. For example, when the motion at 2.5 kHz is compared with that at 2.6 kHz, a significant difference in behavior is seen.

The robot resumes predominantly longitudinal motion around the second resonance, though another shuffling gait occurs at this frequency range. If the off-axis motion of robot leg is too small to cause this performance, the change in mode shape caused by the non-uniformity could be a reason for this behavior.

As calculated in section IV A, the robot should shuffle at 1.25 mm/s at 2.5 kHz if shuffling arises solely from small deflection of robot leg. However, the speed of shuffling (50 mm/s) is much higher than predicted by the analytical model based solely on beam bending. Therefore, other factors such as robot body tilting may be important as well. Fig. 8 shows a simulation with the robot body tilting due to leg asymmetries, again at a representative actuation frequency of 1.4 kHz. In the middle plot of Fig. 8, tilting in the y-direction is on average

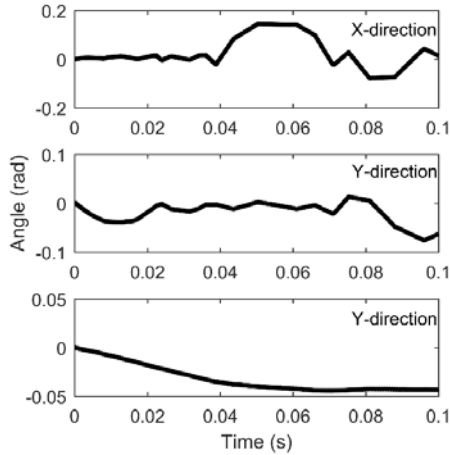


Fig. 8. Robot body tilting simulated in (top) x-direction, (middle) y direction, and (bottom) z-direction, actuation frequency is chosen to be 1.4 kHz.

negative because of the robot non-uniformity. This is evidence that observed leg non-uniformities lead to tilting bias, which may produce faster than anticipated shuffling motion.

## V. DISCUSSIONS AND CONCLUSION

In this paper, we have presented observed steering behaviors from a miniature piezoelectric robot, and have discussed the degree to which such behaviors can be explained by prior dynamic models reported by the authors. While nominal leg deformation behavior can be analyzed by Finite Element Analysis, simple interpretation of resonant frequencies based on beam theory can aid in anticipating variability in locomotion behaviors. Measurement of all six legs in the frequency domain is compared with perturbation analysis, showing that this approach is reasonable for anticipating variability for future design purposes. Adding variability to existing dynamic models by the authors explains variability in longitudinal motion and appearance of turning behaviors of the robot, though with wide margins of error. However, observed “shuffling” gaits away from the resonance remain a puzzle with current understanding of the miniature robot. Two possible causes are proposed as possibly contributing to this shuffling behavior. One is the off-axis motion of the robot leg caused by the tip deflection, and the other one is bias in robot body tilt due to leg asymmetry. From simple analytical calculations, the tip deflection alone cannot result in shuffling of 50 mm/s, so the body tilting from non-uniformity, or possibly changes to mode shapes may be more dominant influences.

In the future, if robot mode shapes and motion types can be identified in a given environment, a controller might use that knowledge to vary robot trajectories on a walking surface with

minimal robot design complexity. A series of forward, shuffling left, backward, shuffling right motion could make the entire walking surface accessible. Further study of the causes of a fast shuffling gait could also better explain observed behavior.

## ACKNOWLEDGMENT

This work was supported by NSF Awards CMMI 1435222 and IIS 1208233. The authors thank Prof. Karl Grosh for providing access to the laser Doppler vibrometer used in testing.

## REFERENCES

- [1] J. Qu, C. B. Teeple, and K. R. Oldham, "Modeling Legged Microrobot Locomotion Based on Contact Dynamics and Vibration in Multiple Modes and Axes," *Journal of Vibration and Acoustics*, vol. 139, p. 031013, 2017.
- [2] J. Qu, J. Choi, and K. R. Oldham, "Dynamic Structural and Contact Modeling for a Silicon Hexapod Microrobot," *Journal of Mechanisms and Robotics*, vol. 9, p. 061006, 2017.
- [3] S. Hollar, A. Flynn, C. Bellew, and K. Pister, "Solar powered 10 mg silicon robot," in *Micro Electro Mechanical Systems, 2003. MEMS-03 Kyoto. IEEE The Sixteenth Annual International Conference on*, 2003, pp. 706-711.
- [4] R. S. Pierre, D. Vogtmann, and S. Bergbreiter, "Model-Based Insights on the Design of a Hexapod Magnetic Walker," in *Experimental Robotics*, 2016, pp. 715-727.
- [5] K. Sugita, D. Tanaka, S. Ono, S. Chiba, K. Iwata, Y. Han, *et al.*, "SMA actuator and pulse-type hardware neural networks IC for fast walking motion of insect-type MEMS microrobot," in *Advanced Intelligent Mechatronics (AIM), 2016 IEEE International Conference on*, 2016, pp. 431-435.
- [6] R. Murthy, A. N. Das, D. O. Popa, and H. E. Stephanou, "ARRIpede: An assembled die-scale microcrawler," *Advanced Robotics*, vol. 25, pp. 965-990, 2011.
- [7] J. H. Ryou and K. R. Oldham, "Dynamic characterization of contact interactions of micro-robotic leg structures," *Smart Materials and Structures*, vol. 23, p. 055014, 2014.
- [8] A. G. Dharmawan, H. H. Hariri, S. Foong, G. S. Soh, and K. L. Wood, "Steerable miniature legged robot driven by a single piezoelectric bending unimorph actuator," in *Robotics and Automation (ICRA), 2017 IEEE International Conference on*, 2017, pp. 6008-6013.
- [9] B. R. Donald, C. G. Levey, C. D. McGray, I. Paprotny, and D. Rus, "An untethered, electrostatic, globally controllable MEMS micro-robot," *Journal of microelectromechanical systems*, vol. 15, pp. 1-15, 2006.
- [10] B. Goldberg, N. Doshi, K. Jayaram, and R. J. Wood, "Gait studies for a quadrupedal microrobot reveal contrasting running templates in two frequency regimes," *Bioinspiration & biomimetics*, vol. 12, p. 046005, 2017.
- [11] N. J. Kohut, D. Zarrouk, K. C. Peterson, and R. S. Fearing, "Aerodynamic steering of a 10 cm high-speed running robot," in *Intelligent Robots and Systems (IROS), 2013 IEEE/RSJ International Conference on*, 2013, pp. 5593-5599.
- [12] N. Kohut, D. Haldane, D. Zarrouk, and R. Fearing, "Effect of inertial tail on yaw rate of 45 gram legged robot," in *Adaptive Mobile Robotics*, ed: World Scientific, 2012, pp. 157-164.
- [13] C. Zhao, K. E. Knisely, and K. Grosh, "Design and fabrication of a piezoelectric MEMS xylophone transducer with a flexible electrical connection," *Sensors and Actuators A: Physical*, 2018.